Microstructure and magnetic properties of oxidized titanium nitride thin films *in situ* grown by pulsed laser deposition

2013 J. Phys. D: Appl. Phys. 46 075002

(http://iopscience.iop.org/0022-3727/46/7/075002)

J. Phys. D: Appl. Phys. **46** (2013) 075002 (7pp) doi:10.1088/0022-3727/46/7/075002

Microstructure and magnetic properties of oxidized titanium nitride thin films *in situ* grown by pulsed laser deposition

S C Chen[1], K Y Sung[1], W Y Tzeng[1], K H Wu[1], J Y Juang[1], T M Uen[1], C W Luo[1], J-Y Lin[2], T Kobayashi[1] and H C Kuo[3]

[1] Department of Electrophysics, National Chiao-Tung University, Hsinchu, Taiwan, Republic of China
[2] Institute of Physics, National Chiao-Tung University, Hsinchu, Taiwan, Republic of China
[3] Department of Photonics and Institute of Electro-Optical Engineering, National Chiao-Tung University, Hsinchu, Taiwan, Republic of China

E-mail: khwu@cc.nctu.edu.tw

Received 6 September 2012, in final form 18 December 2012
Published 23 January 2013
Online at stacks.iop.org/JPhysD/46/075002

Abstract
Different oxidation states of titanium nitride thin films, including pure TiN($h\,0\,0$), $TiN_{1-x}O_x$($h\,0\,0$), Ti_2O_3(0 0 l) and pure anatase TiO_2(0 0 l), were prepared by pulsed laser deposition with various oxygen pressures (P_{O_2}) using a TiN target. Elaborative evolutions of the crystal and electronic structures of the obtained films were examined systematically by x-ray diffraction and x-ray absorption spectroscopy. We found that the Ti_2O_3(0 0 l) film, which was prepared at oxygen pressures $P_{O_2} = 10^{-4}$ Torr, exhibited the maximum room temperature ferromagnetism (RTFM) behaviour. The bound magnetic polaron model is used to clarify the origin of RTFM in these films.

(Some figures may appear in colour only in the online journal)

1. Introduction

Titanium dioxide (TiO_2) thin films have been studied and used extensively [1–6] since they possess remarkable optical, electronic, chemical and mechanical properties such as excellent optical transmittance (>85%) in the visible and near infrared wavelength ranges, high index of refraction ($n \approx 2.35$ at 550 nm), large dielectric constant ($\varepsilon_r \approx 105$ at 4.2 K) and low loss tangent ($\tan\delta \approx 10^{-7}$ at 4.2 K) [7, 8], high chemical stability and mechanical durability. The widespread applications of TiO_2 films include (a) anti-reflecting and protective coating on optical elements; (b) capacitors or gates in microelectronic devices; (c) photocatalyst and catalytic devices; (d) optical waveguide in integrated optics and (e) suitable template layers for growing high-T_c superconducting $YBa_2Cu_3O_7$ (YBCO) films, CrO_2 and $LaSrMnO_3$ films for microwave, biepitaxial junctions and spintronics applications [9–11].

Recently, transition metal-doped and oxygen-deficient TiO_2 films have been demonstrated to exhibit room-temperature ferromagnetic (RTFM) behaviour and thus have attracted extensive interest. In particular, the observation of RTFM in the undoped TiO_2 films has been termed as d^0-magnetism, or magnetism without unpaired d-electrons and is due mostly to defects and/or oxygen vacancies [12–15]. Numerous experimental and theoretical works have been reported ever since to explore the origins of the RTFM in these films. Recently, there were proofs supporting the notion that the existence of local ionic magnetic moment (Ti^{3+}/Ti^{2+} or doped magnetic elements) accompanied by oxygen vacancies might be the origin for the observed magnetic order [12–15], albeit controversial results are not rare and the genuine mechanism responsible for the observed RTFM is still in extensive debate. Therefore, it is crucial to prepare films with various oxygen vacancy concentrations to systematically delineate the effect of oxygen vacancy on the RTFM manifested in the transition metal-free TiO_2 films.

The oxygen-deficient TiO_2 thin films have been prepared with several *in situ* or *ex situ* methods, include (1) *in situ* growth of TiO_2 thin films by pulsed laser deposition (PLD) using the synthesized TiO_2 target under various oxygen partial pressures during deposition [16–18]; (2) *in situ* growth of

TiO_xN_y thin films by direct-current (dc) magnetron sputtering using a metallic Ti target under various pressure ratios of oxygen and nitrogen [19]; (3) *ex situ* nitridation of TiO_2 films, i.e. incorporating nitrogen into the anatase or rutile phase of TiO_2 [20]; (4) *ex situ* oxidation of TiN films, i.e. incorporating oxygen into TiN [21–24]; (5) *ex situ* introducing structural disorder, defects and/or columnar amorphization into TiO_2 films by swift heavy ion irradiation [25]. However, no systematic investigations on the magnetic properties of these films have been carried out.

Previously, epitaxial single-phase rutile or anatase TiO_2 thin films were successfully prepared on (1 0 0)-$SrTiO_3$ (STO) substrates with *in situ* PLD by our group [26]. It was found that, for films deposited on STO(1 0 0) substrates directly using a rutile TiO_2 single crystal target, pure anatase TiO_2(0 0 1) films were obtained even when the substrate temperature (T_s) was higher than 1000 °C. On the other hand, pure rutile TiO_2(1 1 0) films were obtained by *in situ* oxidation of TiN films immediately after they were obtained by PLD. The oxidation temperature was higher than 700 °C with the oxygen pressures (P_{O_2}) being kept at 5 Torr. It is apparent that the specific phases and the preferred orientation of the films obtained under various conditions were mainly determined by the subtle compatibility between the surface and crystalline structures of the substrate (STO), TiN and TiO_2 [26]. In this work, in order to manipulate the oxygen vacancies in titanium oxy-nitride (TiN_xO_y) films, we have deliberately varied the oxygen partial pressure to deposit different TiN_xO_y films, including pure TiN(h 0 0), $TiN_{1-x}O_x$(h 0 0), Ti_2O_3(0 0 l) and pure anatase TiO_2(0 0 l) on the STO(1 0 0) substrate by *in situ* PLD using a TiN target. The evolution of crystalline and electronic structures has been systematically studied by x-ray diffraction (XRD) and x-ray absorption spectroscopy (XAS) measurements. Moreover, the observed changes in film crystalline and electronic structures exhibit intimate correlations with the manifested magnetic properties of these films. We found that the corundum structure of Ti_2O_3(0 0 l) films exhibited the most pronounced room temperature ferromagnetism (RTFM). We infer that formation of the transit structure (Ti_2O_3) may have generated significant amount of oxygen vacancies needed to trigger RTFM. The interactions between the magnetic ions of Ti^{3+} and electrons bound by oxygen vacancies are the fundamental ingredients for forming bound magnetic polaron (BMP) and the percolation of the BMPs at high enough densities would lead to RTFM.

2. Experiments and discussion

2.1. Sample preparation

A KrF excimer laser operating at a repetition rate of 5 Hz with an energy density of 4 J cm^{-2} was used. The target was a hot-pressed TiN (99.9%, purity) pellet. The distance between the target and substrate is 5 cm. The $T_s$was monitored by a thermocouple attached to the substrate holder and was kept at 700 °C during all deposition processes. The background pressure in the chamber was 2×10^{-7} Torr at

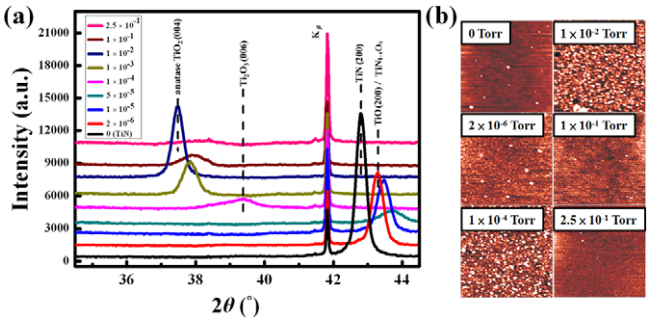

Figure 1. (*a*) The XRD pattern of samples deposited with various oxygen pressures. (*b*) Surface morphologies of samples measured by AFM.

room temperature. As we reported previously [26], the best TiN films were obtained under the background pressure and at T_s = 700 °C, and pure rutile TiO_2 films could be obtained by oxidizing the TiN films at $P_{O_2} > 3.0 \times 10^{-1}$ Torr after deposition. Therefore, in order to systematically investigate the evolution of both the crystalline and electronic structures of the TiN_xO_y films deposited *in situ*, the system was operated at T_s = 700 °C with P_{O_2} being varied in the range 0–0.25 Torr. The thickness of each sample was ~120 nm as determined by an alpha-step profilometer. The areas of all samples are the same as that of the ~0.5 × 0.5 cm^2 STO substrates used for deposition. The crystalline structure of the films was measured by XRD, using Cu $K\alpha$ radiation. The surface morphology of the films was examined by means of atomic force microscopy (AFM). The electronic structure of the TiN_xO_y films was investigated by XAS, using the 6 m high-energy spherical grating monochromatic (6 m-HSGM) beam line at National Synchrotron Radiation Research Center (NSRRC), Taiwan, Republic of China. Moreover, the magnetic property of these samples was measured by a Quantum Design® superconducting quantum interference device (SQUID).

2.2. Crystalline structure

Figures 1(*a*) and (*b*) show the results of XRD and AFM measurements for samples prepared at various oxygen pressures, respectively. As shown in figure 1(*a*), epitaxial TiN(h 0 0) films was grown at T_s = 700 °C and without introducing oxygen (P_{O_2} = 0 Torr) into the chamber during PLD. The $2\theta \approx 42.60°$ diffraction peak assigned to TiN(2 0 0) in figure 1(*a*) corresponds very well to the lattice parameter of 4.24 Å of TiN [26]. When the P_{O_2} was increased slightly (from 2×10^{-6} to 5×10^{-5} Torr), it can be seen that the TiN(2 0 0) diffraction peak starts to shift to higher diffraction angles and the peak width becomes broader with increasing P_{O_2}, as well. This can be understood as follows. With the presence of oxygen during deposition, the nitrogen in pure TiN will be replaced by oxygen due to the higher activity of oxygen. Since the crystal structure of TiN and TiO is the same (B1, rock-salt structure), it is quite natural to conceive that the films are basically consisting of TiN–TiO solid solution, i.e. titanium oxynitride $TiN_{1-x}O_x$. However, the ionic radius of oxygen is smaller than that of nitrogen ion, which in turn might

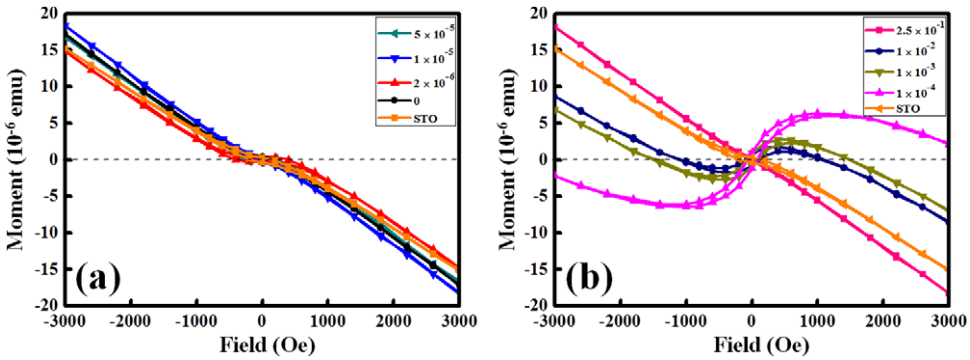

Figure 2. M–H curves measured by SQUID at room temperature (300 K) for the STO substrate and the samples deposited at P_{O_2} (a) from 0 to 5×10^{-5} Torr, (b) from 1×10^{-4} to 2.5×10^{-1} Torr.

lead to the local lattice constant reduction [27]. Consequently, although the diffraction peak appears to remain the same as that of pure TiN(2 0 0), the peak evidently shifts to larger diffraction angles with increasing P_{O_2}. The surface morphology in these films, as demonstrated in AFM images (the top two images of the left column of figure 1(b)), shows the atomically smooth surface with sparsely distributed particulates distributed over the entire image. The root mean square (rms) roughness of the surface was estimated to be about 2 nm, suggesting that the films are indeed remaining as single-phased TiN-TiO solid solution at this stage.

As we further increased the P_{O_2} from 5×10^{-5} to 1×10^{-4} Torr, it is evident that the peak of $TiN_{1-x}O_x$/TiO (2 0 0) disappears gradually and a small, new peak at $2\theta \sim 39.6^\circ$ starts to emerge. This new peak can be indexed to the diffraction peak of Ti_2O_3(0 0 6) (corundum structure). It is noted that the appearance of the Ti_2O_3(0 0 6) peak was also observed by Xu *et al* [28], when using PLD to prepare the anatase TiO_2 films with a Ti target under various P_{O_2}'s [28]. The relatively faint intensity and broadening appearance of this peak indicates that the obtained Ti_2O_3 films should have rather defective and disordered microstructure. However, as will be shown later, this film is, in fact, possessing the most pronounced RTFM among all the samples investigated in this study. This implies that the electronic state of the Ti ions and the large amount of oxygen vacancies in this film may have offered the most favourable environment to give rise to RTFM. When P_{O_2} was further increased to 1×10^{-3} Torr, we found that a diffraction peak corresponding to the metastable anatase TiO_2(0 0 l) structure appeared, which then evolved into a high intensity and sharp XRD peak corresponding to pure anatase TiO_2(0 0 4) diffraction at $P_{O_2} = 1 \times 10^{-2}$ Torr. By further increasing P_{O_2} to 2.5×10^{-1} Torr, the films became amorphous TiO_2. As revealed by AFM images (figure 1(b)), when the growth orientation of the films changes from (h 0 0) to (0 0 l) within the $P_{O_2} = 1 \times 10^{-4}$–$1 \times 10^{-2}$ Torr range, the surface morphology of the films also changes to become more granular with high-density of precipitations over the surface, presumably due to the formation of Ti_2O_3 and anatase TiO_2. The particulates on the surface then disappear at even higher P_{O_2}, reflecting the formation of amorphous TiO_2. All of these surface morphology observations revealed by AFM are quite consistent with the XRD results described above.

2.3. Magnetic property

Figure 2 shows the magnetization (M) versus applied magnetic field (H) curves measured by SQUID at room temperature (300 K) for all samples. The substrate STO and the samples deposited at P_{O_2} values ranging from 0 to 5×10^{-5} Torr (i.e. $TiN_{1-x}O_x$ films) display essentially diamagnetic behaviour (figure 2(a)). On the other hand, as shown in figure 2(b), for the film deposited at $P_{O_2} = 10^{-4}$ Torr, which comprises mainly the corundum Ti_2O_3(0 0 l) structure, a well-defined ferromagnetic hysteresis loop is clearly demonstrated, indicating the existence of pronounced RTFM. The RTFM property, nevertheless, diminishes gradually with further increasing P_{O_2} and disappears completely when P_{O_2} reaches up to 1×10^{-1} Torr at which the TiO_2 films becomes amorphous. These observations strongly suggest that the manifestation of RTFM in these d^0 oxides must be intimately related to the detailed crystalline and electronic structures of the material.

2.4. Electronic structure

The advantage of XAS is its sensitivity to chemical properties and electronic structure of the samples under study. More specifically, analysis of the obtained XAS spectra allows one to discern the unique information on the crystal field strength and symmetry, hybridization, as well as the valence of the specific ion of interest, in this case Ti ions. Thus, in order to elucidate the correlations between the observed magnetic properties and the variation of electronic structures in these TiN_xO_y films deposited under different oxidizing atmospheres, we have systematically measured the O K-edge, Ti $L_{2,3}$-edge, and N K-edge XAS spectra of all the samples.

Figures 3(a) and (b) show the O K-edge and Ti $L_{2,3}$-edge XAS spectra taken in total electron yield (TEY) mode for the as-deposited TiN_xO_y thin films, respectively. The O K-edge XAS spectra reflect the partial density of unoccupied O p states and map, via hybridization, bands of primary Ti character [29]. The spectra of region I (530–536 eV) is attributed to O 2p states hybridized to Ti 3d states. The characteristic XAS peaks for the standard TiO_2 powder are shown in figure 3(c) for comparison. The degenerate Ti 3d band splits into t_{2g} (corresponds to 530.3 eV peak) and e_g (532.9 eV peak) bands due to crystal field effects [30]. This

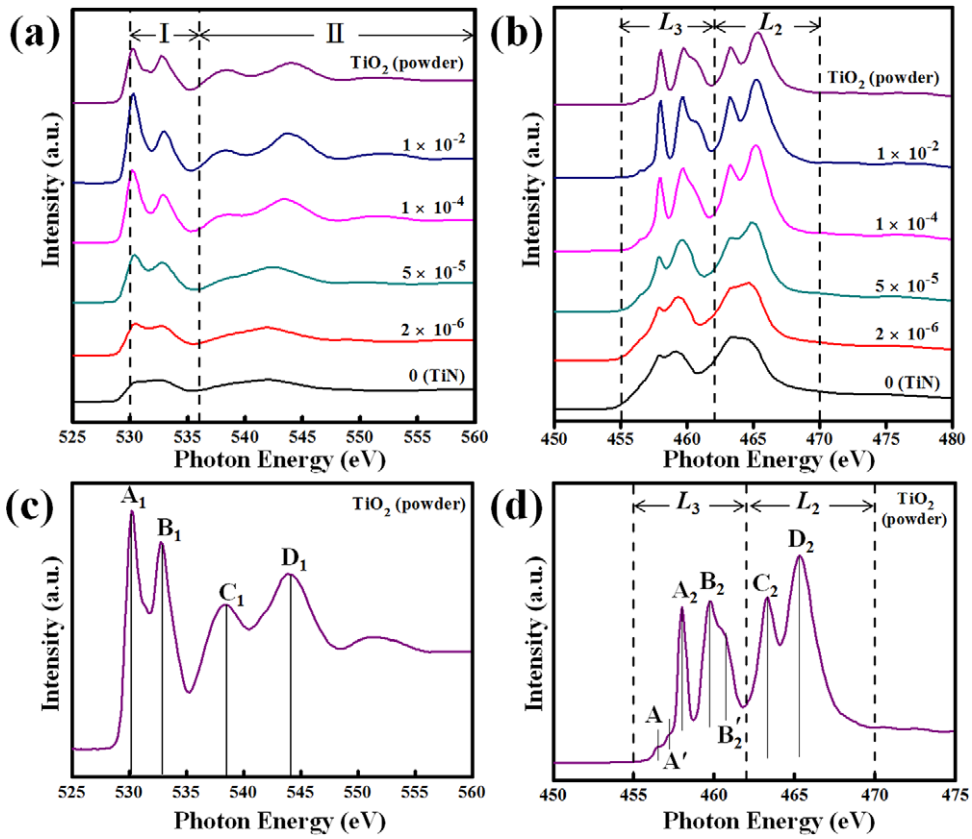

Figure 3. The XAS spectra of (*a*) O *K*-edge, (*b*) Ti $L_{2,3}$-edge for the samples prepared at various oxygen pressures. The characteristic XAS peaks of (*c*) O *K*-edge, (*d*) Ti $L_{2,3}$-edge for standard TiO_2 powder. The incident direction of x-ray is along the normal line of the sample surface. Details explained in the text.

splitting is very sensitive to the coordination number and to the extent of the hybridization. Closer inspection reveals that the t_{2g} and e_g splitting is slightly smaller for samples deposited at lower P_{O_2} ($P_{O_2} < 5 \times 10^{-5}$ Torr), which could be attributed to weaker Ti 3d–O2p interactions caused by the presence of oxygen vacancies and other defects in $TiN_{1-x}O_x$ and Ti_2O_3 films. On the other hand, peaks C_1 and D_1 in region II (>537 eV) are attributed to O 2p states hybridized to Ti 4sp bands [31, 32]. This region exhibits larger dispersion effects and is more sensitive to long-range order [29]. Similar to the peaks in region I, the spectra in this region demonstrate that the t_{2g} and e_g splitting becomes smaller and the Ti 4sp region is shifted towards lower energies for the samples deposited at lower P_{O_2} (<5×10^{-5} Torr). This indicates that the Ti–O interaction in $TiN_{1-x}O_x$ is much weaker than that in Ti_2O_3 and anatase TiO_2 due to lack of long-range order. Finally, we also noted that the O *K*-edge XAS signals are existent even in the TiN powder and the as-deposited TiN thin films, suggesting that a native oxidation layer may exist at the surface of these TiN samples [29].

The XAS spectra of Ti $L_{2,3}$-edge display a considerably more complex structure, which is caused by the combination of atomic interaction and crystal field effects [33, 34]. Figure 3(*b*) shows the XAS spectra of Ti $L_{2,3}$-edge for the TiN_xO_y samples and figure 3(*d*) exhibits the characteristic XAS peaks for the standard TiO_2 powder. The region L_3 and L_2 correspond to O $2p_{3/2}$-Ti 3d and O $2p_{1/2}$-Ti 3d transitions, respectively. For both L_2 and L_3 edges, the crystal field splits the 3d band into t_{2g} (A_2, C_2) and e_g(B_2, D_2) bands. Since the Ti $e_g$orbitals point directly towards the 2p orbitals of the surrounding O atoms, the $e_g$band is very sensitive to the local environment. Moreover, the e_g-related peak of the L_3-edge further splits into two peaks, labelled as B_2 and $B_2^{'}$ in figure 3(*d*). Peak $B_2^{'}$, with intensity smaller than that of B_2, is the fingerprint of the anatase TiO_2 [35]. As shown in figure 3(*c*), when the films deposited at $P_{O_2} < 5 \times 10^{-5}$ Torr, the XAS spectra of $TiN_{1-x}O_x$ films exhibit the same features to that of TiN, which indicates that both have the same cubic NaCl crystal structure. Perhaps, the most relevant changes in the spectra are occurring in $B_2^{'}$ peak. The broadening of the peaks and the disappearance of the shoulder $B_2^{'}$ may due to the structure distortions and the chemical changes for the films deposited at $P_{O_2} < 5 \times 10^{-5}$ Torr. On the other hand, the splitting of (A_2, B_2) peaks and (C_2, D_2) peaks due to crystal field effects becomes much more distinguishable and peak $B_2^{'}$ also appears when $P_{O_2} > 1 \times 10^{-4}$ Torr [36].

To further delineate the substitution of nitrogen by oxygen in all the samples, we also measured the N *K*-edge XAS in fluorescence yield (FY) mode. Figure 4(*a*) shows the XAS spectra of N *K*-edge. The signals in region (397–404 eV) are attributed to N 2p states hybridized to empty Ti 3d bands [37]. The t_{2g} and e_g peaks split from Ti 3d caused by crystal field effects for the standard TiN sample. The spectra for the films deposited at $P_{O_2} < 5 \times 10^{-5}$ Torr exhibit the same features

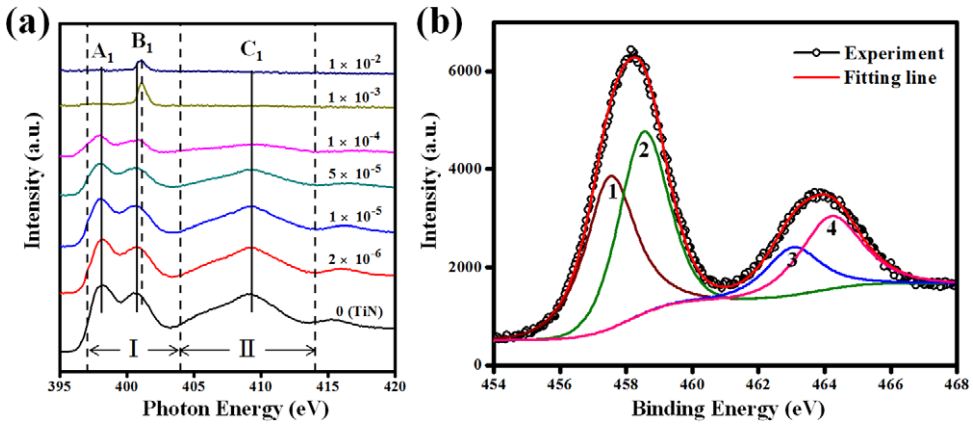

Figure 4. (*a*) The XAS spectra of N *K*-edge for samples deposited under different oxygen pressures. (*b*) The XPS spectrum of Ti_2O_3($P_{O_2} = 1 \times 10^{-4}$ Torr).

except the intensity decreases gradually. This indicates clearly that these $TiN_{1-x}O_x$ films present a closed chemical similarity with TiN. The most relevant changes in the spectra occur in the position and magnitude of the e_g peak. The e_g characteristic peak for TiN locates at 400.7 eV, which appears to shift to 401.4 eV for the sample prepared at $P_{O_2} = 1 \times 10^{-4}$ Torr. This peak grows even further and completely dominates the spectrum when $P_{O_2} > 1 \times 10^{-3}$ Torr and has been generally attributed to unbounded nitrogen [38], that is, the nitrogen atoms still remaining and occupying interstitial positions in the TiO_2 matrix. For the sample deposited at $P_{O_2} > 1 \times 10^{-2}$ Torr, it is evident that all the N *K*-edge signals included this peak disappeared completely, indicating that the nitrogen atoms migrate towards the surface and are thermally desorbed.

From what is described above, it is apparent that both the XRD and XAS results gave consistent account on the crystalline phases and the associated electronic structures evolution of the TiN_xO_y thin films deposited at various oxygen pressures. Briefly, it can be summarized as follows: (1) for the films deposited at $P_{O_2} < 5 \times 10^{-5}$ Torr, the nitrogen in pure TiN will be replaced by oxygen and form the TiN–TiO solid solution, i.e. titanium oxynitride $TiN_{1-x}O_1$. Then the films gradually turns into titanium monoxide (TiO) phase. Since both TiN and TiO are of cubic NaCl structure, the orientation of the films remains the same. (2) For the films deposited at P_{O_2} between 5×10^{-5} and 1×10^{-4} Torr, the crystal structure changes from the NaCl structure (TiO) to the corundum structure (Ti_2O_3) with accompanying changes in preferred orientations. (3) When P_{O_2} further increased to 1×10^{-3} Torr, the metastable anatase TiO_2 (0 0 *l*) structure starts to emerge and an intensive and sharp diffraction peak corresponding to pure anatase TiO_2(0 0 4) is observed at $P_{O_2} = 1 \times 10^{-2}$ Torr. Finally, the crystalline phase TiO_2 transforms to amorphous by further increasing P_{O_2} up to 2.5×10^{-1} Torr.

The question remaining to be answered is how do such crystalline phases and associated electronic structures correlate with the observed RTFM manifestations? As shown in figure 1(*a*), the relative faint and broad XRD peak of Ti_2O_3(0 0 6) indicates that a large amount of oxygen vacancies as well as structural defects maybe introduced when the phase transition involves two phases with drastically different crystal structures, such as during the transition between the NaCl structure (TiO) and corundum structure (Ti_2O_3) with $P_{O_2} \approx 5 \times 10^{-5}$–$1 \times 10^{-4}$ Torr. Nevertheless, it is also the regime where the most pronounced RTFM was observed. Thus, in order to further explore the possible correlations among the RTFM, amount of oxygen vacancies, and the valence of Ti ions in a particular sample, the Ti 2p x-ray photoelectron spectroscopy (XPS) was performed. Figure 4(*b*) displays the Ti 2p XPS spectrum of the Ti_2O_3 film deposited at $P_{O_2} = 1 \times 10^{-4}$ Torr. It is clear that the measured profile is composed of four peaks (labelled as peaks 1–4). The split energy between peaks 2 and 4 is about 5.8 eV, which corresponds very well to the characteristic Ti $2p_{3/2}$ (458.6 eV) and Ti $2p_{1/2}$ (464.4 eV) spin doublet of Ti^{4+} and is consistent with the value measured by Murata *et al* [39]. On the other hand, it is not trivial to precisely distinguish the origin of peaks 1 (457.4 eV) and 3 (463.2 eV). These two peaks may correspond to $2p_{3/2}$ and $2p_{1/2}$ of Ti^{3+} or Ti^{2+} and/or core level peaks of Ti ions bound to oxygen vacancies [40–43]. It is reasonable to conjecture that both Ti^{3+} ions and oxygen vacancies may exist simultaneously in this unique Ti_2O_3 films. In this case, the origin of RTFM can be explained by the BMP model [44, 45]. In the undoped Ti oxides, Ti^{3+} and Ti^{2+} ions can provide the local magnetic moment similar to that provided by the 3d transition metals (Mn, Co and Fe, etc) doped in TiO_2 [46–49]. Meanwhile, the oxygen vacancies will induce slight lattice distortion in the anatase structure and act as both electron donors and electron traps. Then the localized electrons exhibit exchange interaction with the d-shell of Ti^{3+} or Ti^{2+} ions within a localization radius, leading to the formation of BMP with a large net magnetic moment. If the density of the oxygen vacancy is large enough and the 'region' of individual BMP overlaps, the exchange interaction between percolated BMPs would give rise to the ferromagnetic behaviour. It is noted that, within this scenario, for the samples prepared with $P_{O_2} < 5 \times 10^{-5}$ Torr, although there also exist Ti^{3+} or Ti^{2+} in the $TiN_{1-x}O_1$ films, the crystalline structure remains the same cubic NaCl structure and no significant vacancy generation is introduced. As a result, no global RTFM was observed. On the other hand, for the samples prepared at $P_{O_2} = 1 \times 10^{-4}$–$1 \times 10^{-2}$ Torr, the films become Ti_2O_3 and oxygen-deficient

anatase TiO_2, respectively. In this case, a large amount of oxygen vacancies, structural defects accompanied with Ti^{3+} or Ti^{2+} ions exist in these thin films and macroscopic RTFM is observed. At $P_{O_2} > 1 \times 10^{-2}$ Torr, stoichiometric TiO_2 films with Ti^{4+} are formed and the films become non-magnetic, again.

3. Conclusion

In summary, we have prepared TiN_xO_y thin films by PLD with various P_{O_2} using a TiN target. Elaborative evolutions of the crystalline and electronic structures of these films were examined systematically by XRD and XAS measurements. The results indicated that with increasing oxygen partial pressure introduced into the PLD system during deposition, the films evolved sequentially from TiN, TiN–TiO solid solution, TiO, corundum Ti_2O_3, anatase TiO_2 and finally became amorphous at the highest P_{O_2} (∼0.25 Torr) practiced. The magnetic property of these samples measured by SQUID revealed that there exist strong correlation between the RTFM behaviour and the crystalline and electronic structures of the obtained TiN_xO_y films. We found that only the $Ti_2O_3(0\,0\,l)$ and oxygen-deficient anatase TiO_2 films, which were prepared with $P_{O_2} = 1 \times 10^{-4}$ to 1×10^{-2} Torr, exhibited the RTFM behaviour. The XAS and XPS results suggest that the origin of RTFM behaviour is intimately related to the generation of a large amount of oxygen vacancies and magnetic Ti^{3+} or Ti^{2+} ions under the deposition conditions where dramatic structure transformation occurred. The interactions between Ti^{3+}/Ti^{2+} and the electrons bounded by the oxygen vacancies produce high density of BMPs. The percolation of the BMPs thus leads to the observed macroscopic RTFM behaviour. In contrast, for the films deposited at relative low ($P_{O_2} < 1 \times 10^{-4}$ Torr) or high pressures ($P_{O_2} > 1 \times 10^{-2}$ Torr), due to either insufficient oxygen-defects or the absence of Ti^{3+}/Ti^{2+} ions, only diamagnetic behaviour was observed.

Acknowledgments

This work is financially sponsored by the National Science Council (Grant No NSC98-2112-M-009-006-MY3) and the Ministry of Education of Taiwan, R.O.C., under MOE ATU program operated at NCTU.

References

[1] Weinberger B and Garber R 1995 *Appl. Phys. Lett.* **66** 2409
[2] Vorotilov K, Orlova E and Petrovsky V 1992 *Thin Solid Films* **207** 180
[3] Brown W D and Grannemann W W 1978 *Solid-State Electron.* **21** 837
[4] Glassford K M and Chelikowsky J R 1992 *Phys. Rev.* B **46** 1284
[5] Perry A and Pulker K 1985 *Thin Solid Films* **124** 323
[6] Chambers S A 2000 *Surf. Sci. Rep.* **39** 105
[7] Parker N J, Kharel P, Powell J R, Smith P A, Evans P D and Porch A 1999 *IEEE Trans. Appl. Supercond.* **9** 1928
[8] Zuccaro C, Ghosh I, Urban K, Klein N, Penn S and Alford N M 1997 *IEEE Trans. Appl. Supercond.* **7** 3715
[9] Lin P I, Liu C W, Hsieh C C, Wu K H, Juang J Y, Uen T M, Lin J Y and Gou Y S 2001 *Japan J. Appl. Phys.* **40** L377
[10] Liu S J, Lin J Y, Juang J Y, Wu K H, Uen T M and Gou Y S 2002 *Appl. Phys. Lett.* **80** 4202
[11] Liu S J, Chen S F, Juang J Y, Lin J Y, Wu K H, Uen T M and Gou Y S 2003 *Japan J. Appl. Phys.* **42** L287
[12] Rumaiz A K, Ali B, Ceylan A, Boggs M, Beebe T and Shah S I 2007 *Solid State Commun.* **144** 334
[13] Hong N H, Sakai J, Poirot N and Brizé V 2006 *Phys. Rev.* B **73** 132404
[14] Yoon S D, Chen Y, Yang A, Goodrich T L, Zuo X, Arena D A, Ziemer K, Vittoria C and Harris V G 2006 *J. Phys.: Condens. Matter* **18** 355
[15] Pammaraju C D and Sanvito S 2005 *Phys. Rev. Lett.* **94** 217205
[16] Durand H A, Brimaud J H, Hellman O, Shibata H, Makita Y, Gesbert D and Meyrueis P 1995 *Appl. Surf. Sci.* **86** 122
[17] Garapon C, Champeaux C, Mugnier J, Panczer G, Marchet P, Catherijot A and Jacquier B 1996 *Appl. Surf. Sci.* **96** 836
[18] Kim J H, Lee S and Im H S 1999 *Appl. Surf. Sci.* **151** 6
[19] Wei X, Skomski R, Balamurugan B, Sun Z G, Ducharme S and Sellmyer D J 2009 *J. Appl. Phys.* **105** 07C517
[20] Drera G, Mozzati M C, Galinetto P, Diaz-Fernandez Y, Malavasi L, Bondino F, Malvestuto M and Sangaletti L 2010 *Appl. Phys. Lett.* **97** 012506
[21] Wittmer M, Naser J and Melchior H 1981 *J. Appl. Phys.* **52** 6659
[22] Braic M, Balaceanu M, Vladescu A, Kiss A, Braic V, Epurescu G, Dinescu G, Moldovan A, Birjega R and Dinescu M 2007 *Appl. Surf. Sci.* **253** 8210
[23] Chiaramonte T, Cardoso L P, Gelamo R V, Fabreguette F, Sacilotti M, Marco de Lucas M C, Imhoff L, Bourgeois S, Kihn Y and Casanove M-J 2003 *Appl. Surf. Sci.* **212–213** 661
[24] Vaz F, Cerqueira P, Rebouta L, Nascimento S M C, Alves E, Goudeau Ph and Riviere J P 2003 *Surf. Coat. Technol.* **174–175** 197
[25] Thakur H, Kumar R, Thakur P, Brookes N B, Sharma K K, Singh A P, Kumar Y, Gautam S and Chae K H 2011 *J. Appl. Phys.* **110** 083718
[26] Hsieh C C, Wu K H, Juang J Y and Uen T M 2002 *J. Appl. Phys.* **92** 2518
[27] Zajac A T, Radecka M, Zakrzewska K, Brudnik A, Kusior E, Bourgeois S, Macro de Lucas M C and Imhoff L 2009 *J. Power Sources* **194** 93
[28] Xu Y and Shen M R 2009 *Appl. Phys.* A **94** 275
[29] Soriano L, Abbate M, Fuggle J C, Prieto L, Jimenez C, Sanz J M, Galan L and Hofmann S 1993 *J. Vac. Sci. Technol.* A **11** 47
[30] Magnuson M, Mattesini M, Li S, Höglund C, Beckers M, Hultman L and Eriksson O 2007 *Phys. Rev.* B **76** 195127
[31] Brydson R, Sauer H, Engel W, Thomas J M, Zeitler E, Kosugi N and Karuda H 1989 *J. Phys: Condens. Matter* **1** 797
[32] de Groot F M F, Figueiredo M O, Basto M J, Abbate M, Petersen H and Fuggle J C 1992 *Phys. Chem. Miner.* **19** 140
[33] de Groot F M F, Fuggle J C, Thole B T and Sawatzky G A 1990 *Phys. Rev.* B **41** 928
[34] de Groot F M F, Fuggle J C, Thole B T and Sawatzky G A 1990 *Phys. Rev.* B **42** 5459
[35] Krüger P 2010 *Phys. Rev* B **81** 125121
[36] Crocombette J P and Jollet F 1994 *J. Phys: Condens. Matter* **6** 10811
[37] Pflüger J, Fink J, Crecelius G, Bohnen K P and Winter H 1982 *Solid State Commun.* **44** 489
[38] Esaka F, Furuya K, Shimada H, Imamura M, Matsubayashi N, Sato H, Nishijima A, Kawana A, Ichimura H and Kikuchi T 1997 *J. Vac. Sci. Technol.* A **15** 2521
[39] Murata M, Wakino K and Ikeda S 1975 *J. Electron Spectrosc.* **6** 459

[40] Kumar P M, Badrinarayanan and Sastry M 2000 *Thin Solid Films* **358** 122
[41] Sanjines R, Tang H, Berger H, Gozzo F, Margaritondo G and Levy F 1994 *J. Appl. Phys.* **75** 2945
[42] Li Y, Hwang D S, Lee N H and Kim S J 2005 *Chem. Phys. Lett.* **404** 25
[43] Wang X P, Yu Y, Hu X F and Gao L 2000 *Thin Solid Films* **371** 148
[44] Coey J M D, Venkatesan M and Fitzgerald C B 2005 *Nature Mater.* **4** 173
[45] Kaminiski A and Sarma S D 2002 *Phys. Rev. Lett.* **88** 247202
[46] Patel S K S, Gajbhiyea N S and Dateb S K 2011 *J. Alloys. Compounds* **509** 427
[47] Patel S K S and Gajbhiye N S 2011 *Solid State Commun.* **151** 1500
[48] Yan W, Sun Z, Pan Z, Liu Q, Yao T, Wu Z, Song C, Zeng F, Xie Y, Hu T and Wei S 2009 *Appl. Phys. Lett.* **94** 042508
[49] Patel S K S and Gajbhiye N S 2012 *Mater. Chem. Phys.* **132** 175